Neutrophils Obstructing Brain Capillaries Are a Major Cause of No-Reflow in Ischemic Stroke

El Amki, Mohamad ; Glück, Chaim ; Binder, Nadine ; Middleham, William ; Wyss, Matthias T ; Weiss, Tobias ; Meister, Hanna ; Luft, Andreas ; Weller, Michael ; Weber, Bruno ; Wegener, Susanne

Abstract: Despite successful clot retrieval in large vessel occlusion stroke, 50% of patients have an unfavorable clinical outcome. The mechanisms underlying this functional reperfusion failure remain unknown, and therapeutic options are lacking. In the thrombin-model of middle cerebral artery (MCA) stroke in mice, we show that, despite successful thrombolytic recanalization of the proximal MCA, cortical blood flow does not fully recover. Using in vivo two-photon imaging, we demonstrate that this is due to microvascular obstruction of 20%-30% of capillaries in the infarct core and penumbra by neutrophils adhering to distal capillary segments. Depletion of circulating neutrophils using an anti-Ly6G antibody restores microvascular perfusion without increasing the rate of hemorrhagic complications. Strikingly, infarct size and functional deficits are smaller in mice treated with anti-Ly6G. Thus, we propose neutrophil stalling of brain capillaries to contribute to reperfusion failure, which offers promising therapeutic avenues for ischemic stroke.

DOI: https://doi.org/10.1016/j.celrep.2020.108260

Cell Reports

Neutrophils Obstructing Brain Capillaries Are a Major Cause of No-Reflow in Ischemic Stroke

Graphical Abstract

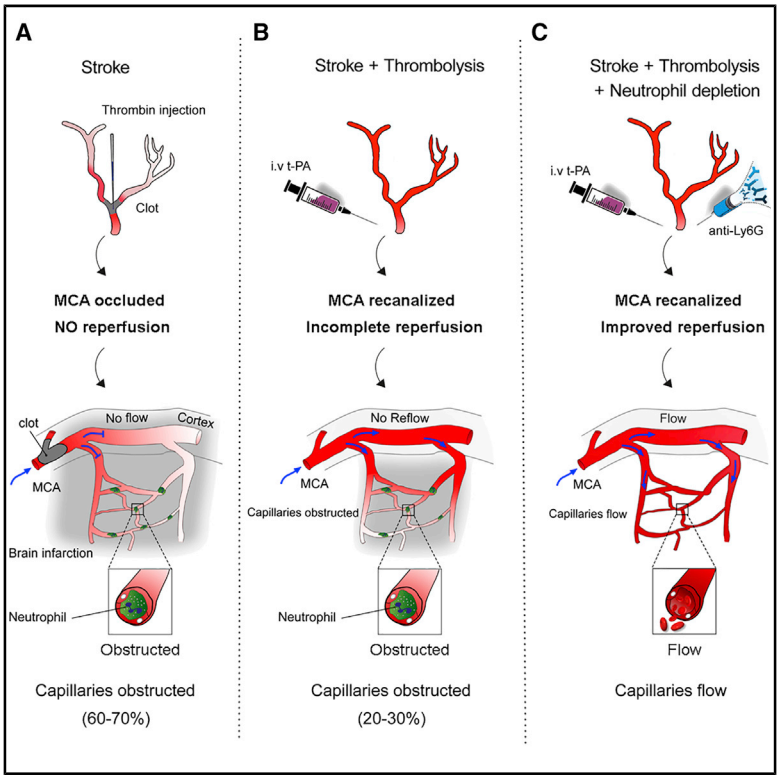

Highlights

- Reperfusion failure despite clot retrieval leads to unfavorable outcome in stroke
- In the thrombin model of stroke, ≈30% capillaries remain occluded after thrombolysis
- Capillaries are plugged by neutrophils, hindering blood flow
- Neutrophil depletion facilitates capillary reperfusion and stroke recovery

Authors

Mohamad El Amki, Chaim Glück, Nadine Binder, ..., Michael Weller, Bruno Weber, Susanne Wegener

Correspondence

bweber@pharma.uzh.ch (B.W.), susanne.wegener@usz.ch (S.W.)

In Brief

In ischemic stroke, thrombolysis does not prevent reperfusion failure of the distal microvascular network. El Amki et al. find that microvascular dysfunction after thrombolysis is caused by neutrophils stalling in capillaries. Using a neutrophil-depleting antibody, they reinstate capillary flow and improve outcome. Treatments for stroke could target microvascular "no-reflow."

El Amki et al., 2020, Cell Reports *33*, 108260
October 13, 2020
https://doi.org/10.1016/j.celrep.2020.108260

Cell Reports

CellPress
OPEN ACCESS

Report

Neutrophils Obstructing Brain Capillaries Are a Major Cause of No-Reflow in Ischemic Stroke

Mohamad El Amki,[1,3] Chaim Glück,[2,3] Nadine Binder,[1] William Middleham,[1] Matthias T. Wyss,[2] Tobias Weiss,[1] Hanna Meister,[1] Andreas Luft,[1] Michael Weller,[1] Bruno Weber,[2,4,*] and Susanne Wegener[1,4,5,*]

[1]Department of Neurology, University Hospital and University of Zurich, and Zurich Neuroscience Center, Zurich, Switzerland
[2]Experimental Imaging and Neuroenergetics, Institute of Pharmacology and Toxicology, University of Zurich, and Zurich Neuroscience Center, Zurich, Switzerland
[3]These authors contributed equally
[4]These authors contributed equally
[5]Lead Contact
*Correspondence: bweber@pharma.uzh.ch (B.W.), susanne.wegener@usz.ch (S.W.)
https://doi.org/10.1016/j.celrep.2020.108260

SUMMARY

Despite successful clot retrieval in large vessel occlusion stroke, ~50% of patients have an unfavorable clinical outcome. The mechanisms underlying this functional reperfusion failure remain unknown, and therapeutic options are lacking. In the thrombin-model of middle cerebral artery (MCA) stroke in mice, we show that, despite successful thrombolytic recanalization of the proximal MCA, cortical blood flow does not fully recover. Using *in vivo* two-photon imaging, we demonstrate that this is due to microvascular obstruction of ~20%–30% of capillaries in the infarct core and penumbra by neutrophils adhering to distal capillary segments. Depletion of circulating neutrophils using an anti-Ly6G antibody restores microvascular perfusion without increasing the rate of hemorrhagic complications. Strikingly, infarct size and functional deficits are smaller in mice treated with anti-Ly6G. Thus, we propose neutrophil stalling of brain capillaries to contribute to reperfusion failure, which offers promising therapeutic avenues for ischemic stroke.

INTRODUCTION

Stroke remains the primary cause of disability worldwide (Benjamin et al., 2019; GBD 2016 Neurology Collaborators, 2019). To date, intravenous thrombolysis with recombinant tissue plasminogen activator (t-PA) and catheter-based mechanical thrombectomy are the pillars of acute stroke therapy (Campbell et al., 2019). Recanalization of occluded vessels enhances oxygen and nutrient delivery to affected tissue, thus facilitating functional recovery from stroke (Panni et al., 2019). However, there is accumulating evidence that clot removal and vessel recanalization do not always go along with tissue reperfusion, a phenomenon called "no-reflow" (Dalkara and Arsava, 2012; Espinosa de Rueda et al., 2015; Soares et al., 2010). No-reflow in stroke refers to microvascular reperfusion failure and tissue damage despite successful recanalization of the larger occluded artery. The no-reflow phenomenon has not only been described in stroke, but also occurs in ischemic heart disease, representing a major obstacle to tissue and functional recovery (Allencherril et al., 2019; del Zoppo and Mabuchi, 2003). Why microvascular no-reflow occurs in stroke even after successful recanalization is poorly understood, and strategies to counteract this perfusion failure do not exist.

Here, we measured distal capillary flow after recanalization in mice subjected to stroke to identify the extent and the underlying mechanisms of the no-reflow phenomenon. We used a thrombin model of stroke and thrombolysis (El Amki et al., 2012; Orset et al., 2007) where a fibrin rich clot is induced in the MCA, which is later dissolved by intravenous t-PA infusion, closely mimicking the clinical scenario of ischemic stroke and intravenous thrombolysis.

RESULTS

No-Reflow in the Thrombin Model of Stroke

To characterize the degree and timing of reperfusion and no-reflow after thrombolysis, we monitored cortical perfusion using laser speckle contrast imaging (LSI) during stroke and thrombolysis with either t-PA or saline (control treatment) for 2 h (Figures 1A–1L). Thrombolysis was administered at 30 min after ischemia onset, which resembles an early treatment time window with high chances of successful recanalization (Orset et al., 2016). Thrombin injection led to successful occlusion of the MCA at its M2 segment bifurcation. At the end of the 2-h observation time, complete recanalization was achieved with t-PA in all treated mice (Figure 1C). None of the saline-treated mice showed complete clot dissolution: partial recanalization occurred in 77.7%, whereas the MCA remained completely occluded in 22.3% (Figure 1C). Clot formation induced a steep drop in perfusion within the core of the lesion, and moderate hypoperfusion in the penumbra. Although there was some degree of spontaneous reperfusion in controls, t-PA treatment significantly raised reperfusion level to 61% ± 4.9% compared to 44% ± 3.5% in the core region (Figures 1G–1I) and 71% ±

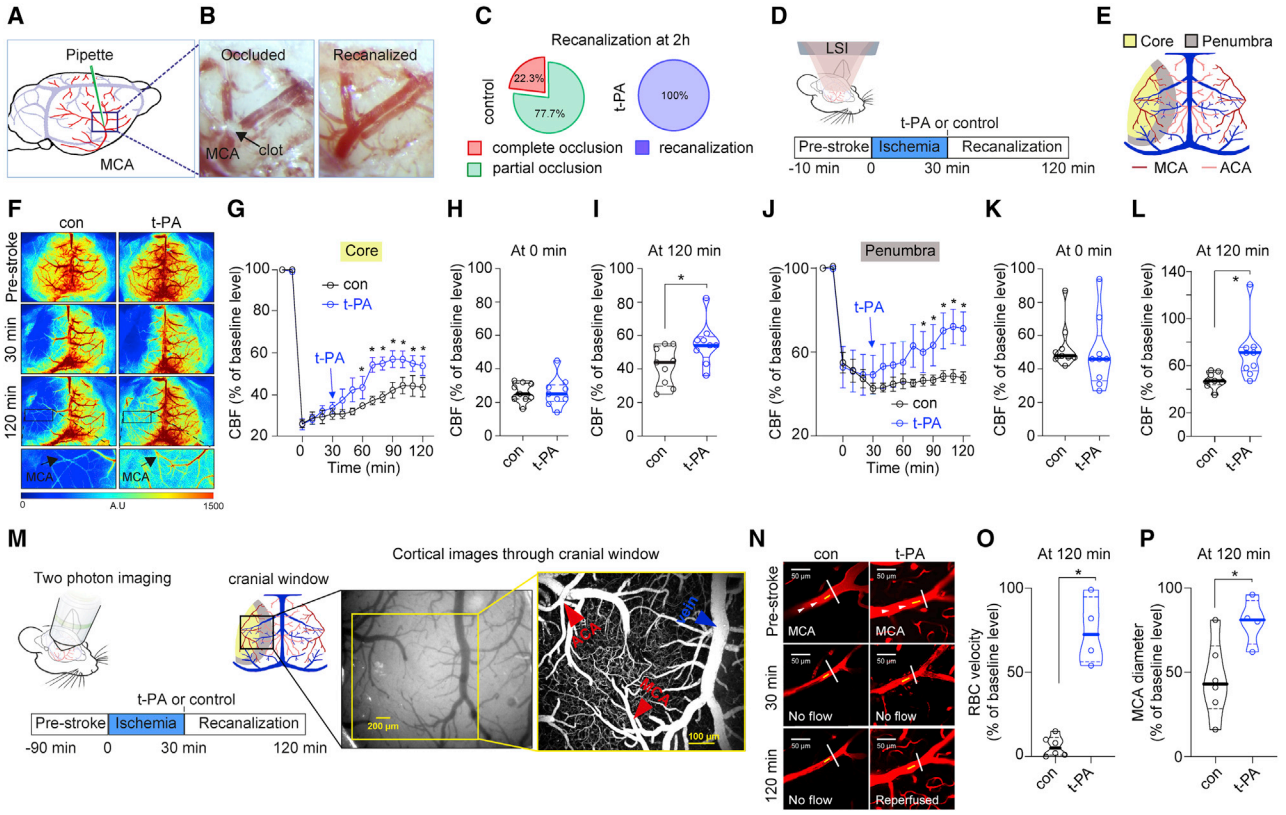

Figure 1. No-Reflow in the Thrombin Model of Stroke

(A) Schematic view of thrombin injection into the middle cerebral artery (MCA)-M2 segment.

(B) Representative images showing the MCA occluded by a clot (left) and recanalized after clot dissolution (right).

(C) Quantitation of MCA clot dissolution at 2 h after stroke in control (saline, left) and t-PA-treated (right) mice (n = 9/group).

(D) Timeline of laser speckle imaging (LSI) experiments.

(E) Schematic drawing of the LSI view on pial vessels and regions of interest (ROIs) used for analyses in (G)–(L).

(F) Representative LSI images showing cortical perfusion from control and t-PA mice at different time points after stroke. The small window (bottom) depicts the MCA branch and surrounding tissue at 120 min after stroke. The color bar indicates perfusion in arbitrary units (a.u.).

(G) LSI recordings for the core ROI compared to baseline in controls or t-PA mice, n = 9/group, *p < 0.05, two-tailed Mann-Whitney U-test.

(H and I) Single values of residual CBF (% of baseline level) in the core ROI for time points 0 and 120 min are shown with violin plots. The thick horizontal line indicates the median value and the dashed horizontal line indicates the quartile values. n = 9/group, *p < 0.05, two-tailed t test.

(J) LSI recordings for the penumbra ROI compared to baseline in controls or t-PA mice, n = 9/group, *p < 0.05, two-tailed Mann-Whitney U-test.

(K and L) Single values of residual CBF (% of baseline level) in the penumbra ROI for time points 0 and 120 min are shown with violin plots. n = 9/group, *p < 0.05, two-tailed t test.

(M) Timeline of two-photon experiments. The position of the cranial window is depicted with the black square in the schematic, covering the core and penumbra ROIs. Scale bar, 200 µm. On the right are a micrograph and *in vivo* two-photon image over the cranial window. Scale bar, 100 µm.

(N) Representative two-photon images depicting the main trunk of the MCA for a control and t-PA-treated mouse, recorded pre-stroke, at 30 and 120 min post-stroke. White (diameter) and yellow (velocity) lines indicate the respective paths for line scans. Scale bar, 50 µm.

(O and P) Quantification of RBC velocity and diameter change at 120 min post-stroke compared to the pre-stroke measurement (% change) are shown with violin plots. n = 6 for controls and n = 4 for t-PA mice; *p < 0.05; two-tailed t test.

7.9% versus 47% ± 2.7% in the penumbra (Figures 1J–1L). Notably, even with thrombolysis and complete clot dissolution, tissue reperfusion was far from complete. Considerable no-reflow was evident beyond the core of the lesion, extending into the penumbra.

To identify changes in vessel diameter and blood flow underlying the no-reflow phenomenon, we imaged the affected distal (pial) MCA segments, using two-photon imaging, and confirmed a profound reduction in red blood cell (RBC) velocity along with a vasoconstriction to 46% ± 11.2% of pre-stroke diameter in saline-treated controls (Figure 1N-P). In t-PA-treated animals, RBC velocity within the distal MCA segment was restored to 80% ± 6.9% of baseline, whereas ischemia-induced MCA diameter reduction was attenuated (74% ± 10%).

We further analyzed cortical vascular networks to identify potential obstacles to reperfusion within the more distal capillary bed in the lesion core as well as the penumbra. To eliminate the possibility that capillary stalls are simply due to adjacent large vessel occlusion, we confirmed that the occluding clot in the MCA-M2 was completely resolved before starting the

measurements (60 min after t-PA; Figures S1A and S1B). We identified patent and stalled capillaries using two-photon microscopy by the presence or absence of streaking RBCs (Figures 2A and 2B; Video S1). Unbiased sampling of cortical vasculature in 12 mice without stroke for 2 h revealed that spontaneous obstruction of capillaries was relatively rare (14 in 2,245 capillaries; ~0.64%, see Figures S1C–S1E).

Capillaries Remain Stalled after Recanalization of the MCA

We observed that after stroke and despite thrombolysis (no obstructions in arterioles), ~35% of capillaries in the core and ~15% of capillaries in the penumbra remained stalled (Figures 2D and 2E). We found stalled capillary segments of 4–10 μm diameter throughout a cortical depth of 300 μm. As cause of capillary stalling after stroke, we identified cells of 8–10 μm diameter resembling neutrophils, as confirmed by dual staining with Rhodamine 6G and Hoechst 33342 (Figure 2G; Video S1 and S4). Neutrophils started to drift along arterioles and venules immediately after ischemia induction, clogging smaller capillaries, thus leading to flow arrest (Videos S2 and S3). Stall points with neutrophils were counted as points where the first cell blocking the flow in an occluded capillary was a neutrophil (Figures 2G–2I; Video S4). Due to labeling and the direct visualization of stall morphology, in addition to stalls caused specifically by neutrophils, we were also able to discriminate between platelet aggregates or RBCs (Figures 2G–2J and S2). We found that after stroke, capillary stalls could be due to neutrophils, RBCs, and even platelet aggregates (Figures 2P and 2Q). Interestingly, after thrombolysis, the majority of stalled capillary segments were due to neutrophil clogging (~75% in the core and ~60% in the penumbra) (Figures 2P and 2Q).

Depletion of Neutrophils with Anti-Ly6G Antibody Reduces Capillary Stalls after Recanalization

To prove that neutrophils stalling capillaries contributed significantly to the no-reflow phenomenon, we applied the monoclonal anti-Ly6G antibody, which specifically depletes neutrophils (Daley et al., 2008), to a separate group of mice 24 h before stroke induction. Flow cytometry analysis confirmed that antibody treatment diminished circulating neutrophils by 97.5% (Figures 3A and 3B). In anti-LyG6-treated mice, we found fewer capillary stall points within the core (5.1%) and the penumbra (2.7%) after stroke (Figure 3C). Strikingly, anti-Ly6G reduced capillary stalls caused by neutrophils and RBCs (Figures 3D–3G). We observed that in the few remaining stalled capillaries after anti-Ly6G treatment, the majority was caused by RBCs (Figures 3J and 3K).

We then tested whether depleting neutrophils improved capillary flow and tissue perfusion, thereby reducing tissue damage. Treatment with anti-Ly6G antibody and t-PA thrombolysis significantly increased tissue reperfusion confirming the causal link between capillary stall and no-reflow (Figures 4A–4D). There was no difference in MCA constriction, but RBC velocity improved in the distal branches of the MCA (Figures 4E and 4F). Importantly, we found reduced ischemic tissue damage at day 7 after stroke in mice treated with anti-Ly6G antibody compared to control mice (Figure 4G). Finally, we evaluated whether mice that received the anti-Ly6G treatment showed a favorable outcome. Indeed, sensorimotor function assessed by sticky tape test was better after stroke in Ly6G-treated mice (Figures 4I–4L), while there was a trend for better performance in the neurological score (Figures 4M and 4N). Hemorrhagic transformation of ischemic stroke is a complication associated with large infarctions, which is more frequent after systemic thrombolysis (Emberson et al., 2014). Although all animals treated with t-PA showed some evidence of hemorrhagic infarct transformation in their brains after reperfusion, this was strongly reduced in animals pre-treated with anti-Ly6G (28.5%) (Figures 4H and S3). To exclude a systemic effect of the antibody on stroke severity independent of thrombolysis, we treated another group of mice subjected to stroke but no t-PA with the anti-Ly6G antibody. We found no improvement in cerebral blood flow, lesion volume, or neurological outcome (Figure S4) in anti-Ly6G pre-treated mice without thrombolysis, suggesting that neutrophils, specifically, are associated with reflow and capillary stalls after recanalization.

DISCUSSION

Fast and efficient recanalization strategies for stroke patients have evolved over the last years (Campbell et al., 2019). However, the microvascular no-reflow is a major problem for successful tissue reperfusion and recovery from stroke.

Using LSI and two-photon imaging, we confirm that microvascular no-reflow impairs tissue reperfusion after stroke in mice. Despite successful large vessel recanalization through thrombolysis, stalling of ~20%–30% of capillaries in the distal vascular network by neutrophils limited tissue reperfusion to only ~60% of baseline. Therefore, intravenous thrombolysis with t-PA only partially restores perfusion of brain tissue distal to the occlusion site. We found areas with no-reflow extending beyond the severely hypoperfused (core) area reaching into the ischemic border zone (penumbra).

The no-reflow of brain microvascular networks after ischemia was already described in 1968 (Ames et al., 1968). It is likely that multiple mechanisms contribute to the microvascular no-reflow phenomenon, including endothelial cell dysfunction, embolization of clot fragments into more distal vessel segments, or death in "rigor" of pericytes (El Amki and Wegener, 2017; Hall et al., 2014; Hartings et al., 2017; Ito et al., 2011; Wiseman et al., 2014; Yemisci et al., 2009; Zhang et al., 1999). In the 1980s, leukocyte plugs were first observed in capillaries and smaller post-capillary venules after stroke *ex vivo*, but the functional role in stroke pathophysiology was not clear (Aspey et al., 1989; del Zoppo et al., 1991). Subsequent studies reported leukocyte rolling and accumulation in brain venules, arterioles, and capillaries after ischemia/reperfusion in filament models of stroke using intravital fluorescence microscopy (Ishikawa et al., 1999; Ritter et al., 2000) and suggested that leukocyte adhesion and rolling could contribute to reperfusion failure after stroke (del Zoppo et al., 1991). In a recent study, Erdener et al. (2020) detected an increased number of stalled capillaries in peri-infarct regions in a model of mechanical, distal MCA occlusion using optical coherence tomography, which confirms our findings. However, it was not possible to differentiate between different

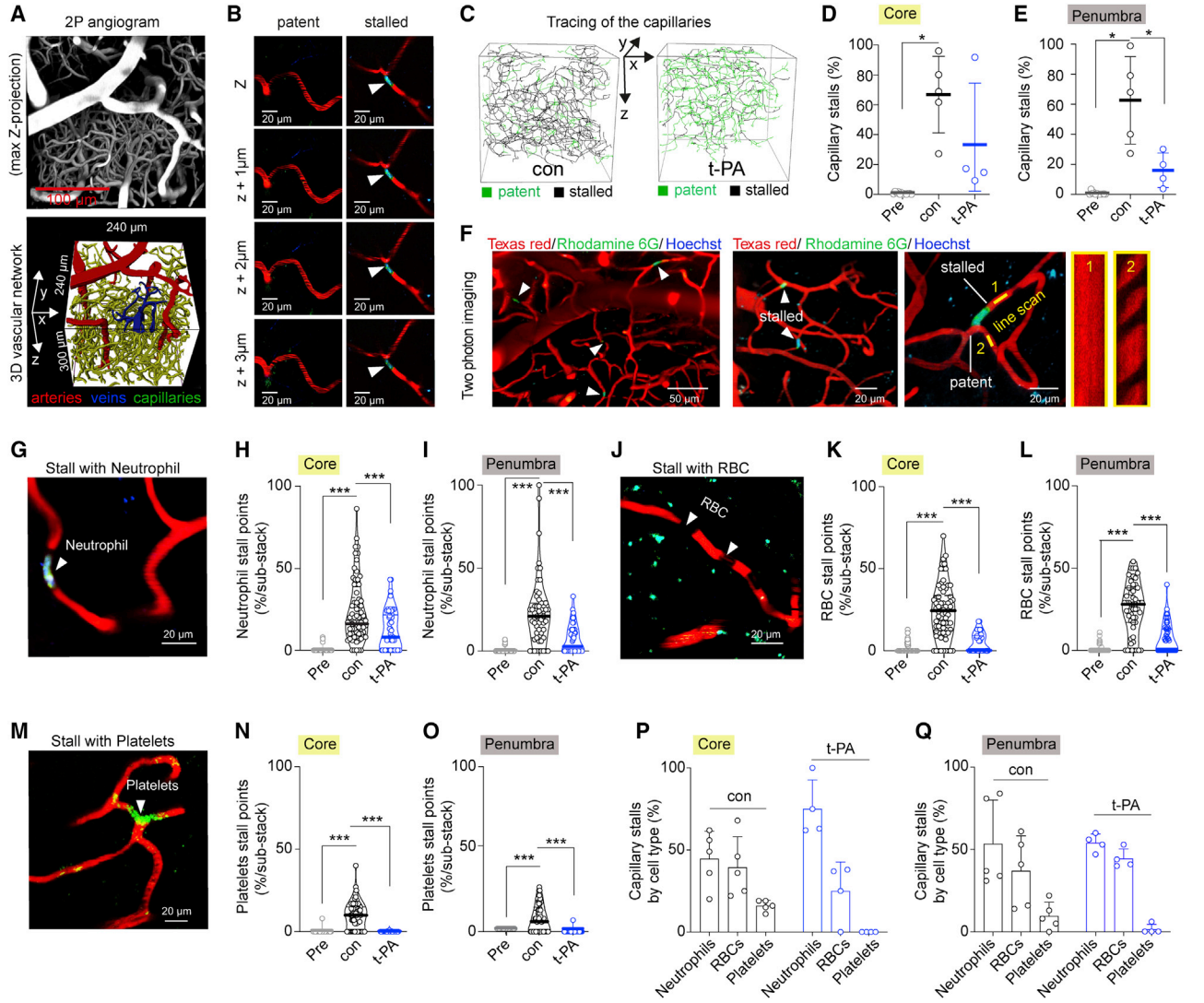

Figure 2. Capillaries Remain Stalled after Recanalization of the MCA

(A) Two-photon microscopy angiogram of the cortex with a penetrating arteriole branch of the MCA, shown as maximum Z-projection. Scale bar, 100 µm. Below, the reconstructed 3D vascular network from the z stack (240 × 240 × 300 µm^3) of the angiogram following image segmentation (x,y,z image), with vessels color-coded based on classification (red, arteries; blue, veins; green, capillaries).

(B) Representative two-photon images of capillary segments either patent or stalled (white arrowhead points to a stall). Flow in capillaries was identified by black streaks generated by passing RBCs. Scale bar, 20 µm.

(C) Tracing of capillaries within the 3D vascular network after exclusion of arteries and veins. Left: control. Right: t-PA-treated mouse.

(D and E) Quantification of capillary stalls in the core and penumbra ROIs, comparing pre-stroke (~6,700 capillaries; n = 11 mice), control (~1,850 capillaries; n = 5 mice), and t-PA (~1,430 capillaries; n = 4 mice)-treated groups. *p < 0.05, two-tailed t test.

(F) Representative two-photon images of capillary segments either stalled (white arrowheads) or patent. Scale bar, 50 µm. Flow in capillaries was identified by streaks generated by passing RBCs and is confirmed by line scan measurements (yellow lines, 1 is stalled and 2 patent; most right panels). Dual staining with Rhodamine 6G (green) and Hoechst 33342 (blue) allows for the differentiation between neutrophils and platelets.

(G, J, and M) Representative images of a stall caused by neutrophils (G), RBCs (J), or platelets (M) distinguished by fluorescence labels and morphology. Scale bar, 20 µm.

(H, I, K, L, N, and O) Quantification of neutrophil stalls (H and I), RBC stalls (K and L), and platelet stalls (N and O) in the core and penumbra ROIs for pre-stroke, control, and t-PA groups, displayed as violin plots. Individual points show % of stall points per sub-stack (240 × 240 × 20 µm^3). *p < 0.05, two-tailed t test.

(P and Q) Percentages of capillaries stalled specifically with neutrophils, RBCs, or platelets in the core and penumbra ROI for control (n = 5) and t-PA-treated mice (n = 4). (P) From the total number of stalled capillaries in the core of control mice (66% stalled capillaries shown in D), neutrophils were responsible for 47% of the stalls, RBCs were responsible for 43% of stalls, and platelets aggregates were responsible for 10% of the stalls. In the 33% of stalled capillaries in the core of t-PA-treated mice shown in (D), neutrophils were responsible of 67% of the stalls, and RBCs were responsible for 33% of the stalls, whereas none of the capillaries were stalled because of platelets. (Q) From the stalled capillaries in the penumbra of control mice (62%), 53% of the stalls were due to neutrophils, 37% due to RBCs, and 10% due to platelets aggregates. From the stalled capillaries in the penumbra of t-PA mice (16%), 54% of the stalls were due to neutrophils, 44% due to RBCs, and 2% due to platelets aggregates.

CellPress
OPEN ACCESS

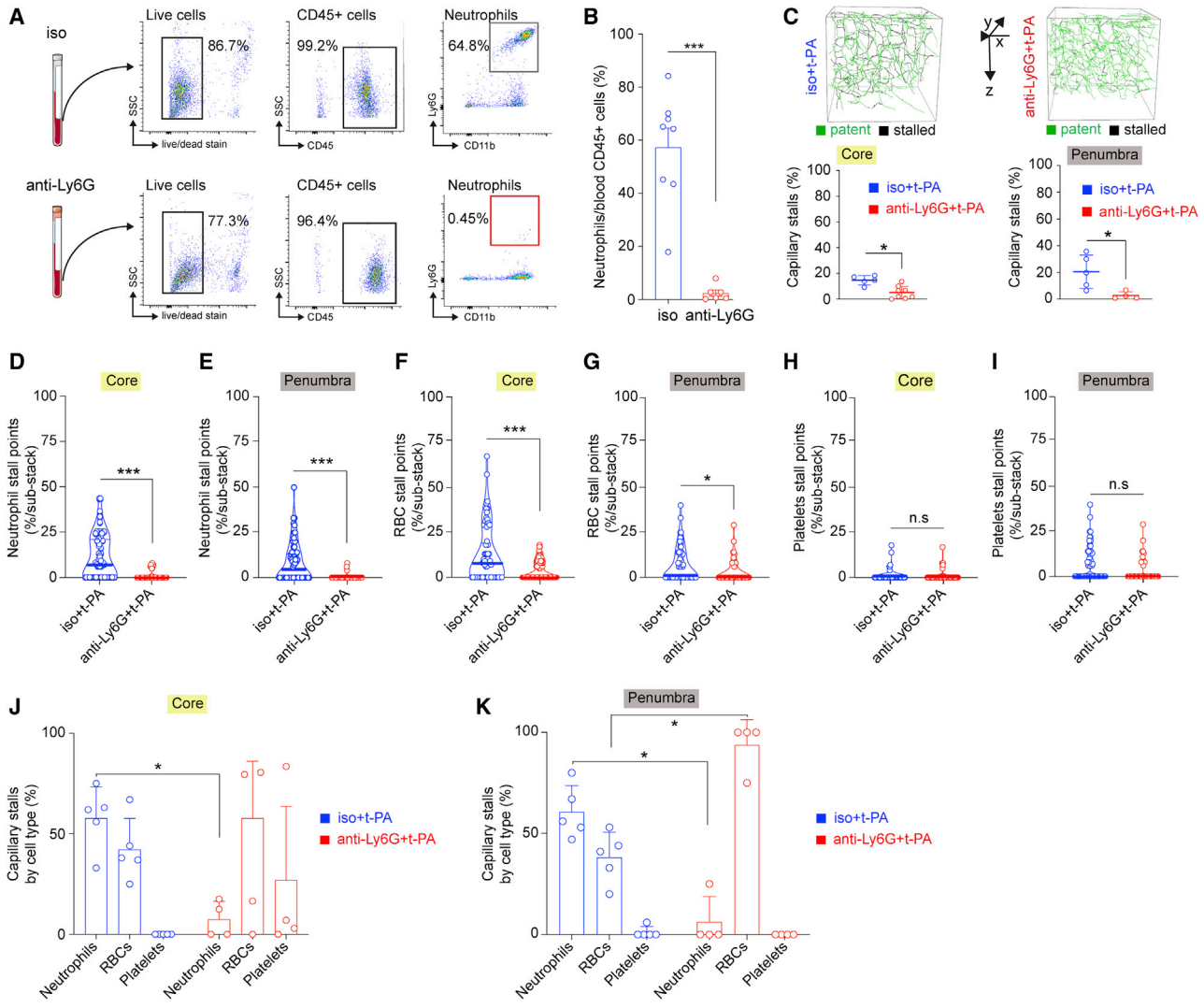

Figure 3. Depletion of Neutrophils with Anti-Ly6G Antibody Reduces Capillary Stalls after Recanalization

(A) Flow cytometry gating for blood neutrophils. Representative flow cytometry dot plots demonstrating the gating strategy to detect neutrophils ($Ly6G^+$ $CD11b^+$ population) from n = 14 mice 24 h after treatment with anti-Ly6G antibody or control isotope (iso) antibody. Numbers above the quadrants indicate percentage of gated events.

(B) Quantification of flow cytometry data for mice treated with anti-Ly6G and isotope antibody. Data from individual mice are plotted, n = 8 for the isotope control group and n = 6 for the anti-Ly6G antibody group, *p < 0.05, unpaired Student's t test.

(C) Upper row: tracing of the vascular network of isotope + t-PA-treated mice (left) and anti-Ly6G + t-PA-treated mice (right), showing stalled capillaries in black. Lower row: quantification of capillary stalls in the core (left) and penumbra (right) ROI, comparing isotope + t-PA-treated groups (~1,750 capillaries; n = 5) and anti-Ly6G + t-PA-treated groups (~2,280 capillaries; n = 4).

(D, F, and H) Violin plots depicting stall points in the core ROI, caused by neutrophils (D), RBCs (F), and platelets (H) in isotope control + t-PA- and anti-Ly6G +t-PA-treated groups. ***p < 0.001, two-tailed Mann-Whitney test.

(E, G, and I) Violin plots depicting stall points in the penumbra ROI, caused by neutrophils (E), RBCs (G), and platelets (I) in isotope control + t-PA- and anti-Ly6G + t-PA-treated groups. ***p < 0.001, two-tailed Mann-Whitney test.

(J and K) Percentages of capillaries stalled specifically with neutrophils, RBCs, or platelets in the core and penumbra ROI for isotope control + t-PA- (n = 5) and anti-Ly6G + t-PA-treated groups (n = 4). (J) From the total number of stalled capillaries in the core of t-PA-treated mice (15% stalled capillaries), 58% of the stalls were due to neutrophils and 42% due to RBCs. In the 5% of stalled capillaries in the core of anti-Ly6G + t-PA-treated mice, neutrophils were responsible of 10% of the stalls, and RBCs were responsible for 59% of the stalls, whereas 31% of the capillaries were stalled because of platelets. (K) From the stalled capillaries in the penumbra of t-PA-treated mice (20%), 59% of the stalls were due to neutrophils, 40% due to RBCs, and 1% due to platelets aggregates. From the stalled capillaries in the penumbra of anti-Ly6G + t-PA-treated mice (2%), 6% of the stalls were due to neutrophils and 94% were due to RBCs.

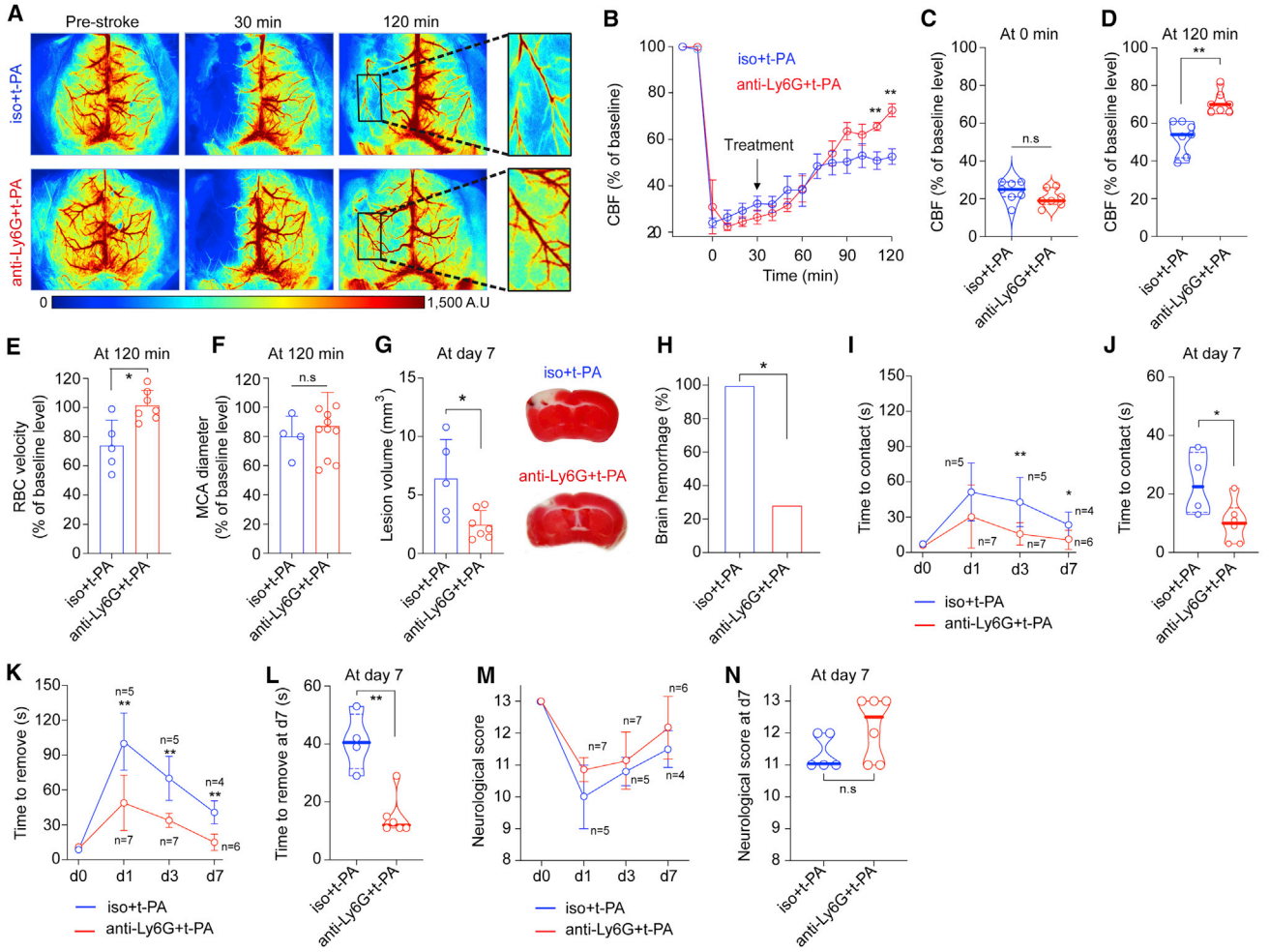

Figure 4. Cortical Reperfusion, Ischemic Damage, and Behavioral Assessment

(A) Representative LSI images showing the cortical perfusion from isotope antibody (iso) + t-PA- and anti-Ly6G + t-PA-treated mice pre-stroke, at 30 min (just before t-PA treatment) and at 120 min. The small window (right) depicts the MCA branch and surrounding tissue after treatment. The color bar indicates perfusion in arbitrary units (a.u.).

(B) Graphs showing LSI recordings for the respective ROIs compared to baseline over time; n = 7 mice/group, **p < 0.01, two-tailed Mann-Whitney U-test.

(C and D) Individual values of residual CBF (% of baseline level) for time points 0 and 120 min are shown with violin plots (n = 7 mice/group). **p < 0.01, two-tailed t test.

(E and F) Bar plots for the quantification of line scan measurements. RBC velocity changes (E) and diameter change of the MCA (F). Values for the isotope antibody + t-PA (n = 4) and anti-Ly6G + t-PA (n = 4) were compared to the pre-stroke measurements (2–3 measurements/mouse). *p < 0.05 in nested model t test.

(G) Bar graph depicting infarct volumes from individual mice at day 7. Mice treated with isotope + t-PA (n = 5) and or anti-Ly6G antibody + t-PA (n = 7), *p < 0.05 in two-tailed Mann-Whitney U-test. On the right, two representative TTC-stained brain sections showing lesions (pale) in a mouse with prior isotope (upper) or anti-Ly6G (lower) treatment.

(H) Fraction of mice with intracerebral hemorrhage detected on TTC-stains within 7 days after stroke in isotope- or anti-Ly6G-treated groups.

(I–N) Sticky tape removal and neurological score assessment in isotope antibody + t-PA-treated mice (n = 5) and Ly6G antibody + t-PA-treated mice (n = 7) at days 1, 3, and 7 after stroke. (I, K, and M) *p < 0.05, **p < 0.01, one-way Kruskal-Wallis ANOVA with post hoc Dunn's multiple-comparison correction to compare between groups. Data are mean ± SD (J, L, and N). *p < 0.05, **p < 0.01, two-tailed t test.

sources of capillary stalls or to evaluate their role in thrombolysis, which is a key reperfusion treatment in stroke patients.

The ability to map capillary patency across the cortex during t-PA induced reperfusion allowed the *in vivo* demonstration of microcirculatory stalling and reperfusion failure, in line with previous histological reports (Hallenbeck et al., 1986; Zhang et al., 1999). Rapid upregulation of endothelial adhesion molecules (VCAM1, ICAM1, and P-selectin) during cerebral ischemia is likely involved, leading to an increased endothelium-neutrophil interaction and prolonged adhesion (Reglero-Real et al., 2016). When MCA occlusion is permanent, adhesion molecules are expressed in both core and penumbra (Gauberti et al., 2013). However, in transient stroke models, the increase of VCAM-1 expression may be restricted to the core (C57Bl6 mice) or involve the penumbra (Swiss mice), depending on the extent of collateral network, which is critical for maintaining blood flow in penumbral

areas (El Amki et al., 2018; Zhang and Faber, 2019). BALB/c mice with their poor leptomeningeal collaterals are likely to have a similar inflammatory penumbral phenotype, which may further booster leucocyte stalls.

Recently, clinical studies have provided evidence that elevated blood neutrophil count on admission is a biomarker for unfavorable outcome in stroke patients receiving thrombolysis (Chen et al., 2018; Malhotra et al., 2018). This implies that indeed, neutrophils might be involved in amplifying tissue injury in stroke patients and in other neurological diseases, where chronic hypoperfusion augments neural decay (Cruz Hernández et al., 2019).

When we depleted neutrophils by targeted antibody treatment, tissue reperfusion was substantially improved in both core and penumbra. Importantly, anti-Ly6G treatment led to a pronounced attenuation of stroke-induced damage in our model of thrombin-occlusion and thrombolysis. It resulted in smaller stroke lesion volumes as well as less functional impairment at 7 days after stroke. The beneficial effect of anti-Ly6G treatment was not observed in mice without recanalization (stroke without t-PA thrombolysis), confirming that neutrophil depletion works through enhancement of microvascular perfusion, which requires that flow in the proximal arteries is reinstalled. Given the fact that neutrophils affect the coagulation cascade (Kambas et al., 2012), it is reassuring that, even when treatment was combined with t-PA, we found no increase in hemorrhagic complications or mortality.

While complete depletion of neutrophils is not a feasible treatment option for stroke patients due to their important and multiple roles in neuro-inflammation and repair, our results support the development of therapeutic strategies geared against neutrophil adhesion in stroke. Notably, our data suggest that such treatment concepts appear to be beneficial even in the hyper-acute phase of stroke and combined to the current reperfusion strategies. Because it requires 24 h to achieve neutrophil depletion with the anti-Ly6G antibody (Erdener et al., 2020), this approach is not suited as an acute post-stroke treatment. Furthermore, Ly6G is expressed in mice and not in humans. Therefore, more research is required to identify translational therapeutic drug targets that counteract neutrophil stalling in stroke patients.

One limitation of our proof-of-concept study was inclusion of young animals without co-morbidities present in many stroke patients. In addition, we included only male mice to compare our results to previous work done in this stroke model. We are aware of the neuroanatomical, neurochemical, and developmental differences between sexes. Therefore, sex-related differences in no-reflow after stroke, thrombolysis and anti-Ly6G treatment deserve further investigations.

Taken together, our data provide *in vivo* evidence that by clogging capillaries, neutrophils contribute to stroke morbidity, even after successful thrombolysis and recanalization of the occluded artery. Future concepts that aim to integrate inhibition of neutrophil adhesion to capillaries with thrombolytic approaches are a promising avenue for ischemic stroke therapy.

STAR★METHODS

Detailed methods are provided in the online version of this paper and include the following:

SUPPLEMENTAL INFORMATION

Supplemental Information can be found online at https://doi.org/10.1016/j.celrep.2020.108260.

ACKNOWLEDGMENTS

This study was supported by the Swiss National Science Foundation (SNSF) PP00P3_170683, the Swiss Heart Foundation, and the University of Zurich (Clinical Research Priority Program Stroke).

AUTHOR CONTRIBUTIONS

M.E.A. and C.G. designed and performed experiments and statistical analysis. N.B. performed laser speckle imaging, behavioral analysis and stroke lesions evaluation. W.M. performed vessel segmentation and data analysis. M.T.W. contributed to cranial window preparation and two photon imaging. T.W. and H.M. performed the flow cytometry experiments and analyses. A.L. and M.W. reviewed and edited the manuscript. B.W. and S.W. conceptualized the project, supervised the project, acquired the funding, and reviewed the manuscript. All authors were involved in writing and critically reviewing the manuscript.

DECLARATION OF INTERESTS

The authors declare no competing interests.

Received: March 6, 2020
Revised: August 18, 2020
Accepted: September 21, 2020
Published: October 13, 2020

REFERENCES

Allencherril, J., Jneid, H., Atar, D., Alam, M., Levine, G., Kloner, R.A., and Birnbaum, Y. (2019). Pathophysiology, Diagnosis, and Management of the No-Reflow Phenomenon. Cardiovasc. Drugs Ther. *33*, 589–597.

Ames, A., 3rd, Wright, R.L., Kowada, M., Thurston, J.M., and Majno, G. (1968). Cerebral ischemia. II. The no-reflow phenomenon. Am. J. Pathol. *52*, 437–453.

Aspey, B.S., Jessimer, C., Pereira, S., and Harrison, M.J. (1989). Do leukocytes have a role in the cerebral no-reflow phenomenon? J. Neurol. Neurosurg. Psychiatry *52*, 526–528.

Barrett, M.J.P., Ferrari, K.D., Stobart, J.L., Holub, M., and Weber, B. (2018). CHIPS: an Extensible Toolbox for Cellular and Hemodynamic Two-Photon Image Analysis. Neuroinformatics *16*, 145–147.

Baumgartner, P., El Amki, M., Bracko, O., Luft, A.R., and Wegener, S. (2018). Sensorimotor stroke alters hippocampo-thalamic network activity. Sci. Rep. *8*, 15770.

Benjamin, E.J., Muntner, P., Alonso, A., Bittencourt, M.S., Callaway, C.W., Carson, A.P., Chamberlain, A.M., Chang, A.R., Cheng, S., Das, S.R., et al.; American Heart Association Council on Epidemiology and Prevention Statistics Committee and Stroke Statistics Subcommittee (2019). Heart Disease and Stroke Statistics-2019 Update: A Report From the American Heart Association. Circulation *139*, e56–e528.

Benstaali, C., Mailloux, A., Bogdan, A., Auzéby, A., and Touitou, Y. (2001). Circadian rhythms of body temperature and motor activity in rodents their relationships with the light-dark cycle. Life Sci. *68*, 2645–2656.

Campbell, B.C.V., De Silva, D.A., Macleod, M.R., Coutts, S.B., Schwamm, L.H., Davis, S.M., and Donnan, G.A. (2019). Ischaemic stroke. Nat. Rev. Dis. Primers *5*, 70.

Chen, J., Zhang, Z., Chen, L., Feng, X., Hu, W., Ge, W., Li, X., Jin, P., and Shao, B. (2018). Correlation of Changes in Leukocytes Levels 24 Hours after Intravenous Thrombolysis With Prognosis in Patients With Acute Ischemic Stroke. J. Stroke Cerebrovasc. Dis. *27*, 2857–2862.

Cruz Hernández, J.C., Bracko, O., Kersbergen, C.J., Muse, V., Haft-Javaherian, M., Berg, M., Park, L., Vinarcsik, L.K., Ivasyk, I., Rivera, D.A., et al. (2019). Neutrophil adhesion in brain capillaries reduces cortical blood flow and impairs memory function in Alzheimer's disease mouse models. Nat. Neurosci. *22*, 413–420.

Daley, J.M., Thomay, A.A., Connolly, M.D., Reichner, J.S., and Albina, J.E. (2008). Use of Ly6G-specific monoclonal antibody to deplete neutrophils in mice. J. Leukoc. Biol. *83*, 64–70.

Dalkara, T., and Arsava, E.M. (2012). Can restoring incomplete microcirculatory reperfusion improve stroke outcome after thrombolysis? J. Cereb. Blood Flow Metab. *32*, 2091–2099.

del Zoppo, G.J., and Mabuchi, T. (2003). Cerebral microvessel responses to focal ischemia. J. Cereb. Blood Flow Metab. *23*, 879–894.

del Zoppo, G.J., Schmid-Schönbein, G.W., Mori, E., Copeland, B.R., and Chang, C.M. (1991). Polymorphonuclear leukocytes occlude capillaries following middle cerebral artery occlusion and reperfusion in baboons. Stroke *22*, 1276–1283.

El Amki, M., and Wegener, S. (2017). Improving Cerebral Blood Flow after Arterial Recanalization: A Novel Therapeutic Strategy in Stroke. Int. J. Mol. Sci. *18*, 2669.

El Amki, M., Lerouet, D., Coqueran, B., Curis, E., Orset, C., Vivien, D., Plotkine, M., Marchand-Leroux, C., and Margaill, I. (2012). Experimental modeling of recombinant tissue plasminogen activator effects after ischemic stroke. Exp. Neurol. *238*, 138–144.

El Amki, M., Binder, N., Steffen, R., Schneider, H., Luft, A.R., Weller, M., Imthurn, B., Merki-Feld, G.S., and Wegener, S. (2019). Contraceptive drugs mitigate experimental stroke-induced brain injury. Cardiovasc. Res. *115*, 637–646.

El Amki, M., Lerouet, D., Garraud, M., Teng, F., Beray-Berthat, V., Coqueran, B., Barsacq, B., Abbou, C., Palmier, B., Marchand-Leroux, C., and Margaill, I. (2018). Improved Reperfusion and Vasculoprotection by the Poly(ADP-Ribose) Polymerase Inhibitor PJ34 After Stroke and Thrombolysis in Mice. Mol. Neurobiol. *55*, 9156–9168.

Emberson, J., Lees, K.R., Lyden, P., Blackwell, L., Albers, G., Bluhmki, E., Brott, T., Cohen, G., Davis, S., Donnan, G., et al.; Stroke Thrombolysis Trialists' Collaborative Group (2014). Effect of treatment delay, age, and stroke severity on the effects of intravenous thrombolysis with alteplase for acute ischaemic stroke: a meta-analysis of individual patient data from randomised trials. Lancet *384*, 1929–1935.

Erdener, S.E., Tang, J., Kilic, K., Postnov, D., Giblin, J.T., Kura, S., Chen, I.A., Vayisoglu, T., Sakadzic, S., Schaffer, C.B., et al. (2020). Dynamic capillary stalls in reperfused ischemic penumbra contribute to injury: A hyperacute role for neutrophils in persistent traffic jams. J. Cereb. Blood Flow Metab. Published online April 1, 2020. https://doi.org/10.1177/0271678X20914179.

Espinosa de Rueda, M., Parrilla, G., Manzano-Fernández, S., García-Villalba, B., Zamarro, J., Hernández-Fernández, F., Sánchez-Vizcaino, C., Carreón, E., Morales, A., and Moreno, A. (2015). Combined Multimodal Computed Tomography Score Correlates With Futile Recanalization After Thrombectomy in Patients With Acute Stroke. Stroke *46*, 2517–2522.

Fedorov, A., Beichel, R., Kalpathy-Cramer, J., Finet, J., Fillion-Robin, J.C., Pujol, S., Bauer, C., Jennings, D., Fennessy, F., Sonka, M., et al. (2012). 3D Slicer as an image computing platform for the Quantitative Imaging Network. Magn. Reson. Imaging *30*, 1323–1341.

Gauberti, M., Montagne, A., Marcos-Contreras, O.A., Le Béhot, A., Maubert, E., and Vivien, D. (2013). Ultra-sensitive molecular MRI of vascular cell adhesion molecule-1 reveals a dynamic inflammatory penumbra after strokes. Stroke *44*, 1988–1996.

GBD 2016 Neurology Collaborators (2019). Global, regional, and national burden of neurological disorders, 1990-2016: a systematic analysis for the Global Burden of Disease Study 2016. Lancet Neurol. *18*, 459–480.

Haddad, M., Beray-Berthat, V., Coqueran, B., Palmier, B., Szabo, C., Plotkine, M., and Margaill, I. (2008). Reduction of hemorrhagic transformation by PJ34, a poly(ADP-ribose)polymerase inhibitor, after permanent focal cerebral ischemia in mice. Eur. J. Pharmacol. *588*, 52–57.

Hall, C.N., Reynell, C., Gesslein, B., Hamilton, N.B., Mishra, A., Sutherland, B.A., O'Farrell, F.M., Buchan, A.M., Lauritzen, M., and Attwell, D. (2014). Capillary pericytes regulate cerebral blood flow in health and disease. Nature *508*, 55–60.

Hallenbeck, J.M., Dutka, A.J., Tanishima, T., Kochanek, P.M., Kumaroo, K.K., Thompson, C.B., Obrenovitch, T.P., and Contreras, T.J. (1986). Polymorphonuclear leukocyte accumulation in brain regions with low blood flow during the early postischemic period. Stroke *17*, 246–253.

Hartings, J.A., Shuttleworth, C.W., Kirov, S.A., Ayata, C., Hinzman, J.M., Foreman, B., Andrew, R.D., Boutelle, M.G., Brennan, K.C., Carlson, A.P., et al. (2017). The continuum of spreading depolarizations in acute cortical lesion development: Examining Leão's legacy. J. Cereb. Blood Flow Metab. *37*, 1571–1594.

Holtmaat, A., Bonhoeffer, T., Chow, D.K., Chuckowree, J., De Paola, V., Hofer, S.B., Hübener, M., Keck, T., Knott, G., Lee, W.C., et al. (2009). Long-term, high-resolution imaging in the mouse neocortex through a chronic cranial window. Nat. Protoc. *4*, 1128–1144.

Ishikawa, M., Sekizuka, E., Sato, S., Yamaguchi, N., Inamasu, J., Bertalanffy, H., Kawase, T., and Iadecola, C. (1999). Effects of moderate hypothermia on leukocyte- endothelium interaction in the rat pial microvasculature after transient middle cerebral artery occlusion. Stroke *30*, 1679–1686.

Ito, U., Hakamata, Y., Kawakami, E., and Oyanagi, K. (2011). Temporary [corrected] cerebral ischemia results in swollen astrocytic end-feet that compress microvessels and lead to delayed [corrected] focal cortical infarction. J. Cereb. Blood Flow Metab. *31*, 328–338.

Kambas, K., Mitroulis, I., and Ritis, K. (2012). The emerging role of neutrophils in thrombosis-the journey of TF through NETs. Front. Immunol. *3*, 385.

Malhotra, K., Goyal, N., Chang, J.J., Broce, M., Pandhi, A., Kerro, A., Shahripour, R.B., Alexandrov, A.V., and Tsivgoulis, G. (2018). Differential leukocyte counts on admission predict outcomes in patients with acute ischaemic stroke treated with intravenous thrombolysis. Eur. J. Neurol. *25*, 1417–1424.

Mayrhofer, J.M., Haiss, F., Haenni, D., Weber, S., Zuend, M., Barrett, M.J., Ferrari, K.D., Maechler, P., Saab, A.S., Stobart, J.L., et al. (2015). Design and performance of an ultra-flexible two-photon microscope for in vivo research. Biomed. Opt. Express *6*, 4228–4237.

Maysami, S., Wong, R., Pradillo, J.M., Denes, A., Dhungana, H., Malm, T., Koistinaho, J., Orset, C., Rahman, M., Rubio, M., et al. (2016). A cross-

laboratory preclinical study on the effectiveness of interleukin-1 receptor antagonist in stroke. J. Cereb. Blood Flow Metab. *36*, 596–605.

Orset, C., Macrez, R., Young, A.R., Panthou, D., Angles-Cano, E., Maubert, E., Agin, V., and Vivien, D. (2007). Mouse model of in situ thromboembolic stroke and reperfusion. Stroke *38*, 2771–2778.

Orset, C., Haelewyn, B., Allan, S.M., Ansar, S., Campos, F., Cho, T.H., Durand, A., El Amki, M., Fatar, M., Garcia-Yébenes, I., et al. (2016). Efficacy of Alteplase in a Mouse Model of Acute Ischemic Stroke: A Retrospective Pooled Analysis. Stroke *47*, 1312–1318.

Panni, P., Gory, B., Xie, Y., Consoli, A., Desilles, J.P., Mazighi, M., Labreuche, J., Piotin, M., Turjman, F., Eker, O.F., et al.; ETIS (Endovascular Treatment in Ischemic Stroke) Investigators (2019). Acute Stroke With Large Ischemic Core Treated by Thrombectomy. Stroke *50*, 1164–1171.

Pologruto, T.A., Sabatini, B.L., and Svoboda, K. (2003). ScanImage: flexible software for operating laser scanning microscopes. Biomed. Eng. Online *2*, 13.

Reglero-Real, N., Colom, B., Bodkin, J.V., and Nourshargh, S. (2016). Endothelial Cell Junctional Adhesion Molecules: Role and Regulation of Expression in Inflammation. Arterioscler. Thromb. Vasc. Biol. *36*, 2048–2057.

Ritter, L.S., Orozco, J.A., Coull, B.M., McDonagh, P.F., and Rosenblum, W.I. (2000). Leukocyte accumulation and hemodynamic changes in the cerebral microcirculation during early reperfusion after stroke. Stroke *31*, 1153–1161.

Schaar, K.L., Brenneman, M.M., and Savitz, S.I. (2010). Functional assessments in the rodent stroke model. Exp. Transl. Stroke Med. *2*, 13.

Schmid, F., Barrett, M.J.P., Obrist, D., Weber, B., and Jenny, P. (2019). Red blood cells stabilize flow in brain microvascular networks. PLoS Comput. Biol. *15*, e1007231.

Sekhon, L.H., Spence, I., Morgan, M.K., and Weber, N.C. (1995). Chronic cerebral hypoperfusion in the rat: temporal delineation of effects and the in vitro ischemic threshold. Brain Res. *704*, 107–111.

Soares, B.P., Tong, E., Hom, J., Cheng, S.C., Bredno, J., Boussel, L., Smith, W.S., and Wintermark, M. (2010). Reperfusion is a more accurate predictor of follow-up infarct volume than recanalization: a proof of concept using CT in acute ischemic stroke patients. Stroke *41*, e34–e40.

Wiseman, S., Marlborough, F., Doubal, F., Webb, D.J., and Wardlaw, J. (2014). Blood markers of coagulation, fibrinolysis, endothelial dysfunction and inflammation in lacunar stroke versus non-lacunar stroke and non-stroke: systematic review and meta-analysis. Cerebrovasc. Dis. *37*, 64–75.

Yemisci, M., Gursoy-Ozdemir, Y., Vural, A., Can, A., Topalkara, K., and Dalkara, T. (2009). Pericyte contraction induced by oxidative-nitrative stress impairs capillary reflow despite successful opening of an occluded cerebral artery. Nat. Med. *15*, 1031–1037.

Zhang, H., and Faber, J.E. (2019). Transient versus Permanent MCA Occlusion in Mice Genetically Modified to Have Good versus Poor Collaterals. Med One *4*, e190024.

Zhang, Z.G., Chopp, M., Goussev, A., Lu, D., Morris, D., Tsang, W., Powers, C., and Ho, K.L. (1999). Cerebral microvascular obstruction by fibrin is associated with upregulation of PAI-1 acutely after onset of focal embolic ischemia in rats. J. Neurosci. *19*, 10898–10907.

STAR★METHODS

KEY RESOURCES TABLE

REAGENT or RESOURCE	SOURCE	IDENTIFIER
Antibodies		
anti-Ly6G antibody	BD PharMingen	Cat #551459
rat IgG2a	Thermo Fisher	Cat #02-9688
anti-CD45.1-AF488	Biolegend	Cat #110718
anti-CD11b-BV510	Biolegend	Cat #101245
anti Ly-6G-FITC	Biolegend	Cat #127606
Chemicals, Peptides, and Recombinant Proteins		
fentanyl	Sintetica	Cat #699811
midazolam	Roche	Cat #M-908-1ML
medetomidine	Orion Pharma	Cat # 520370
human alpha-thrombin	Haematologic Technologies	Cat #HCT-0020
2,3,5-triphenyltetrazolium chloride	Sigma-Aldrich	Cat #T8877
Texas red Dextran	Life Technologies	Cat #D-1864
Rhodamine 6G	Sigma Aldrich	Cat #252433
Hoechst 33342	Sigma Aldrich	Cat #B2261
Deposited Data		
CHIPS toolbox for MATLAB	https://github.com/EIN-lab/CHIPS	GitHub
Experimental Models: Organisms/Strains		
BALB/c mice	Charles Rivers	627BALB/cByJ
Software and Algorithms		
ImageJ version 1.41	ImageJ Software	https://imagej.nih.gov/
ScanImage	Pologruto et al., 2003	N/A
Radon algorithm	Schmid et al., 2019	N/A
MATLAB	Mathworks	N/A
3D slicer v4.10.2	3D slicer Software	https://www.slicer.org/
GraphPad Prism v8.0	GraphPad Software	https://www.graphpad.com/

RESOURCE AVAILABILITY

Lead Contact

Further information and request for resources and reagents should be directed to and will be fulfilled by Lead Contact Susanne Wegener (Susanne.Wegener@usz.ch).

Materials Availability Statement

This study did not generate new unique reagents.

Data and Code Availability

CHIPS toolbox for MATLAB is freely available on GitHub (https://github.com/EIN-lab/CHIPS) (Barrett et al., 2018).

EXPERIMENTAL MODEL AND SUBJECT DETAILS

All animal experiments were approved by the local veterinary authorities in Zurich and conformed to the guidelines of the Swiss Animal Protection Law, Veterinary Office, Canton of Zurich (Act of Animal Protection 16 December 2005 and Animal Protection Ordinance 23 April 2008, animal welfare assurance numbers ZH165/19 and ZH224/15). For all experiments, male BALB/c mice (Charles Rivers, no. 028), three to four months old were used. The mice had free access to water and food and an inverted 12-hour light/dark

cycle to perform experiments during the dark (active) phase. Testing during the light phase induces a pronounced behavioral inhibition and rodents perform better during the active phase (Benstaali et al., 2001; Schaar et al., 2010). More specifically, Zeitgeber Time (ZT0) corresponds to the start of the light period, and ZT 12 refers to the start of the dark period. Experiments were performed during the day at ZT 16 to ZT 20 (mid-day). All testing procedures were carried out during the same period for all groups. All animals were randomized for all stroke studies and procedures. All experiments were blinded; the operators responsible for experimental procedure and data analysis were blinded and unaware of group allocation throughout the experiments.

METHOD DETAILS

Anesthesia

For head-post and cranial window implantation, animals were anesthetized intraperitoneally with a mixture of fentanyl (0.05 mg/kg bodyweight; Sintenyl, Sintetica), midazolam (5 mg/kg bodyweight; Dormicum, Roche), and medetomidine (0.5 mg/kg bodyweight; Domitor, Orion Pharma). A facemask provided 100% oxygen at a rate of 300 ml/min. For stroke induction and two-photon imaging, anesthesia was induced with isoflurane 4%, maintained at 1.2% with continuous supply of 300 ml/min 100% oxygen. Core temperature of the animals was kept constant at 37°C using a homeothermic blanket heating system during all surgical and experimental procedures (Harvard Apparatus). The animal‘s head was fixed in a stereotaxic apparatus and the eyes were kept wet with ointment (vitamin A eye cream; Bausch & Lomb).

Head-Post Implantation

A bonding agent (Gluma Comfort Bond; Heraeus Kulzer) was applied to the cleaned skull and polymerized with a handheld blue light source (600 mW/cm^2; Demetron LC). A custom-made aluminum head post was connected to the bonding agent with dental cement (EvoFlow; Ivoclar Vivadent AG) for stable and reproducible fixation in the microscope setup. The skin lesion was treated with antibiotic ointment (Neomycin, Cicatrex; Janssen-Cilag AG) and was closed with acrylic glue (Histoacryl, B. Braun). After surgery, animals were kept warm and received analgesics (buprenorphine 0.1 mg/kg bodyweight; Sintetica).

Cranial window surgery

A 4 × 4 mm craniotomy was performed above the somatosensory cortex (centered above the left somatosensory cortex −3mm from Bregma and 3.5 −4 mm lateral) using a dental drill (Bien-Air). A square coverslip (3 × 3 mm, UQG Optics) was placed on the exposed dura mater and fixed to the skull with dental cement (Holtmaat et al., 2009).

Antibody treatment

Purified anti-Ly6G antibody (BD PharMingen, catalog number 551459) and isotope control antibody rat IgG2a (Thermo Fisher, catalog number 02-9688) were injected intraperitoneally at a dose of 4 mg/kg bodyweight, 24 hours before imaging.

Flow cytometry analysis of blood cells

Flow cytometry staining was performed in staining buffer at 4°C. 200 μl blood was collected from the left cardiac ventricle and stored in heparin-coated vials. RBC were lysed by incubating the blood sample in blood lysis buffer (RBC lysis buffer, eBiosciences) for 15 min at room temperature. Samples were centrifuged (2000 g) for 15 min and the supernatant was discarded. Remaining blood cells were washed twice with PBS. Then, cells were resuspended in cryosolution containing: RPMI, 40% FBS and 10% DMSO and stored at −80°C before FACS analysis. For neutrophils staining, the following antibodies were used: anti-CD45.1-AF488, anti-CD11b-BV510 and anti Ly-6G-FITC (Biolegend). As controls, we used isotope-matched antibodies from Sigma-Aldrich. Acquisition was performed on a BD FACSVerse Analyzer (BD Biosciences) and data were analyzed with FlowJo (TreeStar). Blood and bone marrow leukocyte staining samples were fixed with BD Cytofix (BD Biosciences) and analyzed within 24 h.

Thrombin stroke model

We induced focal cerebral ischemia as described previously (El Amki et al., 2012, 2018; Orset et al., 2007). In brief, mice were fixed in a stereotactic frame, the skin between the left eye and ear was incised and the temporal muscle retracted. After craniotomy and dura excision, a glass pipette (calibrated at 15 mm/μl; Assistant ref. 555/5; Hoechst, Sondheim-Rhoen, Germany) was introduced into the lumen of the MCA and one μl of purified human alpha-thrombin (1UI; HCT-0020, Haematologic Technologies Inc., USA) was injected to induce the formation of a clot *in situ*. The pipette was removed 10 min after thrombin injection. Ischemia induction was considered stable when CBF rapidly dropped to at least 50% of baseline level in the MCA territory (El Amki et al., 2012; Sekhon et al., 1995) and remained below 50% for at least 30 min. Animals without stable ischemia induction were excluded from further experiments.

Laser Speckle Cortical Imaging

Cortical perfusion was monitored before and during ischemia, and throughout the recanalization phase for 120 min with a Laser speckle imaging monitor (FLPI, Moor Instruments, UK). The LSC images are generated with arbitrary units in a 16-color palette by the MoorFLPI software.

T-PA administration

Thirty minutes after induction of ischemia, thrombolysis was initiated via tail vein (200 μl, 1 mg/ml in 0.9% saline) of human t-PA (10 mg/kg, Actilyse, Boehringer Ingelheim) according to previous data (El Amki et al., 2012; Maysami et al., 2016). Ten % were given as a bolus and 90% were perfused at a rate of six μl/min. Control groups received saline instead of t-PA.

Quantification of lesion volume and hemorrhages

After completion of the experiments (day 7), mice were euthanized by receiving an overdose i.p. injection of pentobarbital (200 mg/kg) followed by decapitation. Brains were extracted and cut into 1 mm thick coronal slices from 6.5 to 0.5 mm anterior to the inter-aural line and placed in 2% 2,3,5-triphenyltetrazolium chloride (TTC, cat. #T8877, Sigma-Aldrich, St. Louis, MO) for 10 min at 37°C to delineate infarcts which appear pale in the staining. Infarct areas were determined by a blinded investigator using an image analysis system (ImageJ version 1.41). To correct for brain swelling, each infarct area was multiplied by the ratio of the surface of the intact (contralateral) hemisphere to the infarcted (ipsilateral) hemisphere at the same level. Total volume of damaged tissue, expressed as cubic millimeters, was calculated by linear integration of the corrected lesion areas (El Amki et al., 2019). The presence of hemorrhage was recorded from TTC- stained brain slices at the time of premature death or sacrifice at day 7. Microscopic, macroscopic and total hemorrhagic scores were visually quantified on each level, from TTC- stained brain slices, as previously described (Haddad et al., 2008).

Two-photon imaging

After cranial window implantation, mice were allowed to recover for two weeks prior to two-photon imaging. Imaging was performed using a custom-built two-photon laser scanning microscope (2PLSM) (Mayrhofer et al., 2015) with a tuneable pulsed laser (Chameleon Discovery TPC, Coherent Inc.) equipped with either a 20x (W-Plan-Apochromat 20x/1.0 NA, Zeiss) or 25x (W-Plan-Apochromat 25x/1.0 NA, Olympus) water immersion objective. During measurements, the animals were head-fixed and kept under anesthesia as described above. To visualize the vasculature, Texas red Dextran (5% w/v, 70,000 kDa mw, 50 μl, Life Technologies catalog number D-1864) was injected intravenously in the tail vein. White blood cells were stained with Rhodamine 6G (100 μl of 1.0 mg/ml solution in saline, Sigma Aldrich, catalog number 252433). Nuclei were further stained by Hoechst 33342 (50 μl of 4.8 mg/ml in saline, Sigma Aldrich catalog number B2261). All dyes were injected intravenously 10 minutes before imaging and were excited at 900 nm. Emission was detected with GaAsP photomultiplier modules (Hamamatsu Photonics) fitted with 475/64, 520/50 nm and 607/70 band pass filters and separated by a 506, 560 and 652 nm dichroic mirrors (BrightLine; Semrock). The microscope was controlled by a customized version of ScanImage (r3.8.1; Janelia Research Campus (Pologruto et al., 2003)).

Imaging ROIs were in the areas corresponding to LSI: for the core ROI within the area supplied by the frontal MCA and showing severe CBF drop and for the penumbra ROI showing moderate hypoperfusion within the ACA-supplied regions. Z stacks (x,y,z images) were recorded in the respective areas with 1 μm step size, 512x512 pixels, 0.74 Hz, covering roughly a volume of 240 × 240 × 300 μm^3. Line scan acquisitions were performed at 11.84 Hz, 0.55 μm/pixel and for 12.7 s. Baseline measurements were performed 90 min before induction of ischemia.

Quantification of capillary stalls

The researchers producing these quantifications were blinded to treatment groups. Image analysis of z stacks was performed using ImageJ (NIH, version 1.41). Vessel segments were classified as surface and penetrating arterioles and capillaries, or as ascending and surface venules. All vessels smaller than 10 μm were classified as capillaries. Large-surface arterioles were distinguished from large-surface venules based on morphology: arteries were of smaller diameter, had smoother walls and less tortuosity and tended to branch more symmetrically and in Y-shaped junctions compared to veins (Cruz Hernández et al., 2019). In each z stack, vessel segments visible for 20 frames (30 s) were assessed as to whether RBC streaking occurred. To confirm blockage of a capillary segment, higher magnification frame scans and line scans of the respective vessel segment were acquired. Cells within blood vessels were characterized by morphology and staining with Rhodamine 6G and Hoechst 33342. Blockage by RBCs appeared as black hollows, platelets as accumulation of small green particles, while only neutrophils were cells double stained with Rhodamine 6G and Hoechst 33342 (Cruz Hernández et al., 2019).

Line scans were processed with a custom-designed image processing tool box for MATLAB (Cellular and Hemodynamic Image Processing Suite [Barrett et al., 2018]; R2014b; MathWorks). Vessel diameters were determined at full width half maximum (FWHM) from a Gaussian fitted intensity profile drawn perpendicular to the vessel axis. Capillary flow was determined with the Radon algorithm (Schmid et al., 2019). The same vessels were evaluated before stroke, after stroke and throughout the experiment.

Reconstruction of 3D vascular networks and tracing of capillaries

An example z stack was loaded into 3D slicer (3D Slicer 4.10.2) (Fedorov et al., 2012). The 'Segment Editor' module was used to segment the vessels from the whole image by applying an Otsu threshold. Vessels were classified into three groups; arteries/arterioles, veins/venules and capillaries, by both size of vessel (as described above) and area of image acquisition. A separate file was created for each type vessel and the appropriate vessels were manually segmented and assigned a specific color. Default smoothing effects were applied to all segmentations and a volume rendering of each file provided the 3D image of the segmented data. The example 3D tracing of the capillaries was created with the 'Vascular Modeling Toolkit', specifically using the 'Centerline Computation'

option of this module. 3D rendering of example stacks were loaded and an 'origin seed' was placed on the surface of any vessel. The centerlines for each individual vessel was computed from the 'origin seed', creating the line network. Arteries and veins were excluded from the final 3D tracing.

Motor scoring and behavioral assessment

Sensorimotor function was assessed by an investigator blinded to treatment groups using the adhesive tape removal test as well as a composite observational neurological score before stroke and on days 1,3 and 7 thereafter. For the adhesive tape removal test, two strips of tape (rectangular 0.3 × 0.4 cm) were applied to both forepaws in random order. The time the animals took to contact (sensory function/neglect) and remove (motor function) the tape on both sides (left and right) was recorded. Before stroke, animals were trained to remove both tapes within 10 s (Baumgartner et al., 2018). The neurological score was obtained using a composite grading score as described before (El Amki et al., 2019). A lower score indicates larger neurological deficits, while a score of 13 points indicates no neurological deficit.

QUANTIFICATION AND STATISTICAL ANALYSIS

Data in all groups was tested for normality using D'Agostino-Pearson omnibus normality test. Parametric statistics were used only if the data in all groups in the comparison were normally distributed. Statistical analysis was performed using the GraphPad Prism (version 8.0; GraphPad Software La Jolla, CA, USA). All statistical tests and group size (n) are indicated in the figure legends. To account for multiple observations within the imaged mouse, results from each group were compared using univariate nested model t tests before proceeding with the discriminant analysis. Results were expressed either as mean ± s.e.m. (standard error of mean), or median (interquartile range) in violin plots. Significance ($p < 0.05$) between two groups was calculated using unpaired Student's t test or paired t test for normally distributed data, or with the Mann–Whitney test for data with non-normal distribution.